*Journal of Microelectronics and Electronic Packaging* (2014) **11**, 7-15

ISSN: 1551-4897

# LT-TLPS Die Attach for High Temperature Electronic Packaging

Hannes Greve and F. Patrick McCluskey*

***Abstract*—Low temperature transient liquid phase sintering (LT-TLPS) can be used to form high-temperature joints between metallic interfaces at low process temperatures. In this paper, process analyses and shear strength studies of paste-based approaches to LT-TLPS are presented. The process progression studies include DSC analyses and observations of intermetallic compound (IMC) formation by cross-sectioning. It was found that the sintering process reaches completion after sintering times of 15 min for process temperatures approximately 50°C above the melting point of the low temperature constituent. For the shear studies, test samples consisting of copper dice and copper substrates joined by sintering with a variety of sinter pastes with different ratios of copper and tin have been assessed. A fixture was designed for high temperature enabled shear tests at 25°C, 125°C, 250°C, 400°C, and 600°C. The influence of the ratio of the amount of high melting-point constituent to the amount of low melting-point constituent on the maximum application temperature of the sinter paste was analyzed. Ag20Sn and Cu50Sn pastes showed no reduction in shear strength up to 400°C, and Cu40Sn pastes showed high shear strengths up to 600°C. It was shown that LT-TLPS can be used to form high temperature stable joints at low temperatures without the need to apply pressure during processing.**

***Keywords*—Transient liquid phase sintering, lead free solder, die attach, power electronics, high temperature electronics**

## Introduction

Power electronic systems are increasingly used in harsh applications such as deep well drilling or space exploration where the device and the package must be able to withstand extreme external thermal stresses. Furthermore, growing levels of miniaturization and power densities have led to rising thermal stresses from inside the package as well. This necessitates the development of robust packaging solutions for high-temperature and high-power electronic systems. Whereas conventional power devices have been limited to application temperatures of 125°C [1] due to inherent limitations of silicon (Si) semiconductor materials, the introduction of silicon carbide (SiC) and gallium nitride (GaN) wide bandgap semiconductors extends the range of potential applications to temperatures up to 500°C [2, 3].

The manuscript was received on August 16, 2013; revision received on December 3, 2013; accepted on December 8, 2013

The original version of this paper was presented at IMAPS International Conference and Exhibition on High Temperature Electronics Network (HiTEN), July 8-10, 2013, Oxford, United Kingdom.

CALCE/Department of Mechanical Engineering, Clark School of Engineering, University of Maryland, College Park, Maryland 20742

*Corresponding author; email: mcclupa@umd.edu

Finding an appropriate die attach is a major challenge in the design of reliable high temperature power electronics. Due to its proximity to the major location of power dissipation (i.e., the die), die attach is exposed to high thermal loads. As the interface between a semiconductor material with a low coefficient of thermal expansion (CTE) and a substrate with a significantly higher CTE, it is also subject to mechanical stresses induced by these thermal loads. A reliable die attach technology must ensure high fatigue life at all application temperatures as well as providing high thermal and electrical conductivity.

Conventional die attach solutions are lead solder based. However, initiatives like the restriction on hazardous substances directive (RoHS) limit the application of lead as a material in electronics, reducing the use of lead-based solders. Tin-based solders such as SAC305 are a common alternative to lead-based solders, but their low melting temperatures (217°C for SAC305) compared with their lead-based counterparts (Liquidus temperature of 296°C for Pb5.0Sn2.5Ag) are detrimental to their reliability at elevated temperature levels.

The fatigue life of solder joints is reduced considerably as the homologous temperature $T_h$ is increased. $T_h$ is the ratio of the application temperature ($T$) to the melting temperature ($T_m$) of a material in Kelvin. At temperatures above $T_h \approx 0.4$, time dependent plastic deformation, or creep, is initiated. Furthermore, with increasing temperatures, the yield strength is reduced, facilitating instantaneous plastic deformation. The fatigue life or number of mean cycles to failure ($N_f$) for solder follows the Coffin-Manson relation for low-cycle fatigue

$$N_f = \frac{1}{2}\left(\frac{\Delta\gamma}{2\varepsilon_f'}\right)^{\frac{1}{c}},$$

where $\varepsilon_f'$ is the material-dependent fatigue ductility coefficient, $c$ is the material and temperature dependent fatigue ductility exponent, and $\Delta\gamma$ is the cyclic shear strain range metric [4]. Increases in operating temperature increase $T_h$, which affects $c$ due to increased creep, thus reducing $N_f$. The homologous temperature is therefore a good indicator for the fatigue life of a material system under thermal loads.

Table I gives an overview of the homologous temperatures of several die attach material systems at multiple temperature levels. 125°C indicates the traditional application temperature limit for most of the currently available Si-based devices and temperature limit for many power and thermal cycling tests. 200°C and 250°C are potential application temperatures of interest for SiC and GaN power devices.

doi:10.4071/imaps.394 

Table I
Homologous Temperatures of Die Attach Materials

| Die attach | $T_m$ (°C) | $T_h$ at 125°C | $T_h$ at 200°C | $T_h$ at 250°C |
|---|---|---|---|---|
| SAC305 | 217 | 0.81 | 0.97 | >1[1] |
| Pb5.0Sn2.5Ag | 296 | 0.70 | 0.83 | 0.92 |
| $Ag_3Sn$ | 480 | 0.53 | 0.63 | 0.69 |
| $Cu_6Sn_5$ | 415 | 0.58 | 0.69 | 0.76 |
| $Cu_3Sn$ | 676 | 0.42 | 0.50 | 0.55 |
| Ag | 962 | 0.32 | 0.38 | 0.42 |

It can be seen that tin-based solders show a high $T_h$ even at 125°C, which limits their fatigue life. At 200°C they are already very close to their melting temperature and are no longer feasible for reliable application. High-lead solders, with a melting temperature of approximately 300°C, possess a lower $T_h$ at 125°C than SAC305, but at 200°C and above encounter the same issues. The intermetallic compounds (IMCs) $Ag_3Sn$ and $Cu_6Sn_5$ show a significantly lower $T_h$ compared with the solders. Their $T_h$ at 250°C is similar to that of the high-lead solders, generally referred to as high-temperature solders, at 125°C. The copper-rich $Cu_3Sn$ IMC possesses a low $T_h$ over the whole temperature range, indicating very limited creep behavior. Pure silver joints formed by sintering of nanosilver particles also show a very low $T_h$, due to pure silver's $T_m$ of 962°C.

A material that does not undergo significant plastic deformation during a load cycle will possess an extremely long fatigue life. The stress level at which significant plastic deformation is initiated is called the yield stress $\sigma_y$. It can be found in the literature that $\sigma_y$ for IMCs are approximately one order of magnitude above that of solders or bulk silver [5-8]. The plastic deformation experienced by the IMCs will therefore be much lower than that of these softer materials. It can be concluded that joints formed by LT-TLPS systems introduced here should feature much improved fatigue life under high-temperature conditions.

Two types of materials are generally considered as die attach alternatives in high temperature applications (viz. high-lead solders as mentioned above, or systems based on eutectic gold, e.g., AuSn, AuGe, AuSi). To join metallic surfaces using these die attach materials by standard reflow soldering, the process temperature, $T_p$, has to be significantly higher than $T_m$. Usually a $T_p$ that is 50°C above $T_m$ ensures good joint quality. Yet this leads to considerable thermal and mechanical stress on the electronic package, which can be detrimental to system lifetime. Furthermore, lead-based materials run the risk of legislative restriction, while gold-based systems are inherently extremely costly. Taking these aspects and their limited application temperatures into consideration, it can be seen that such solders possess limited potential for high-power and high-temperature die attach applications.

From a processing point of view, a material system that enables joining at low temperatures but forms joints robust to high temperatures is highly advantageous. Sintering is a technology that possesses this property. Two alternative sintering processes exist.

Solid-state (i.e., solid-solid) sintering joins particles by interdiffusion. The driving force is a reduction of surface energy that occurs as the particles agglomerate and the surface area to volume ratio decreases. Substantial heat and pressure are needed to initiate and accelerate the sintering process.

Sintering of silver particles is the most prominent solid-solid sintering approach in the field of electronic packaging. It was first demonstrated for micrometer-sized particles [9]. Even though joints could be formed at relatively low temperatures, a considerable amount of pressure was required to achieve adequate bonding between the silver particles. The use of nanometer-sized particles reduces the required pressure significantly and it has been demonstrated that reliable sinter joints can be formed with this technology [10, 11]. Disadvantages are the comparably high costs associated with this type of material. Furthermore, silver migration may be a reliability concern with pure silver joints [12].

Transient liquid phase sintering (TLPS), sometimes also referred to as solid liquid interface diffusion bonding (SLID), makes use of a liquid phase that is consumed during processing. A joint is created by IMC formation. An advantage of this approach is that pressure is not required, as the joint densification is facilitated by capillary forces and wetting of solid particles by the liquid phase. Yet, as with sintered silver, the high melting temperature of the TLPS joint after it is formed renders rework of interconnects practically impossible. A detailed analysis of the low-temperature TLPS process is given in the subsequent section.

A multitude of different TLPS systems based on tin or indium as the liquid phase material have been demonstrated, notably (Ag, Au, Cu, Ni)-Sn and (Ag, Au)-In. The majority of research has focused on sintering a layer of low melting-point metal sandwiched in between two layers of a high melting-point metal [13-18]. It has been shown that thin layers can be joined within a relatively short time, but that extended annealing times are needed to increase the sinter joint strength, as shown in Table II. Different types of metallization can be bonded and good joint quality has been demonstrated over a wide range of temperatures during thermal cycling. Yet it is not possible to form joints with a relatively thick layer due to Fick's second law of diffusion, which shows that the length of diffusion is proportional to the square root of time. The process time increases quadratically with increasing thickness of the intermetallic layer. This can lead to process durations impractical for manufacturing electronic components even at relatively high temperatures [19].

Limited research has been conducted on LT-TLPS paste-based systems. It has been shown that solder pastes can be

Table II
Process Parameters and Layer Thicknesses for Selected LT-TLPS Systems

| Reference | TLPS system | Thickness of low-temperature constituent | Process time and temperature |
|---|---|---|---|
| [13] | Au + 80Au20Sn | 2 × 1 μm | 10 min at 315°C |
| [14] | Au + Sn | 2 μm | 5 min at 250°C + 20 min |
| | Au + 80AuSn | 7.5 μm | at 300°C/315°C/350°C |
| [15] | Ag + In | 3 μm | 10 min at 210°C + 6,000 min |
| | Au + In | 3.3 μm | at 400°C |
| [16] | Ag + In | 1.9 μm | 7 min at 206°C + 1,560 min at 145°C |

filled with Cu particles to achieve TLPS bonds [20]. AgIn pastes have also been used to form joints at low temperatures [21]. The joint strength at high temperatures has not yet been assessed in the literature. In this paper we will characterize joint shear strength for Ag20Sn, Cu60Sn, Cu50Sn, and Cu40Sn LT-TLPS sinter joints at temperatures of 25°C, 125°C, 250°C, 400°C, and 600°C. Furthermore, we will demonstrate that the sintering process of these pastes is completed after relatively short processing times, even for thick bond layers.

### *A. Transient Liquid Phase Sinter Pastes*

At least two elements are required to form an LT-TLPS sinter system: Constituent A with a low melting temperature, $T_{m,A}$, and constituent B with a high melting temperature, $T_{m,B}$. When the process temperature, $T_p$, is set so that $T_{m,A} < T_p < T_{m,B}$, A melts and wets B, spreading between the solids by capillary forces, interdiffusing and densifying the joint.

Constituent A forms intermetallic compounds with B at the surface of B, while the concentration of B in the liquid A phase increases. Eventually, the concentration of B in the A-rich areas increases to a point where a phase transformation from liquid to solid occurs. With extended annealing time, the joint completely homogenizes until no concentration gradients are present, as shown in Fig. 1. Upon completion of the phase transformation, the melting temperature of the joint has shifted from $T_{m,A}$ to the higher melting temperature of the IMC. This concept enables the sintering of metallic systems at low process temperatures that are robust to high application temperatures.

Fig. 2 shows a system consisting of pure Sn with a $T_{m,Sn}$ of 232°C and pure Cu with a $T_{m,Cu}$ of 1065°C. As $T_p$ is increased above $T_{m,Sn}$, the Sn melts. Copper starts to dissolve into the liquid. As the Cu concentration increases, the η phase forms, which is the intermetallic compound $Cu_6Sn_5$, with a melting temperature of 415°C. In equilibrium, as shown in Fig. 2, all the L is converted to η below a Sn-concentration of 59.0-60.9%. The η will subsequently begin to transform into the ε phase, which is $Cu_3Sn$, with a melting temperature above 600°C. The transformation to ε with a $T_m > 600$°C is completed for a material with an overall composition of 38.4% Sn or less.

The Ag-Sn system is shown in Fig. 3. The formation of phases is similar to that of the Cu-Sn system. Differences exist in the names of the IMCs, their melting temperatures, and their corresponding high melting temperature constituent concentrations. At a Sn concentration of 26.8 wt.%, a shift of

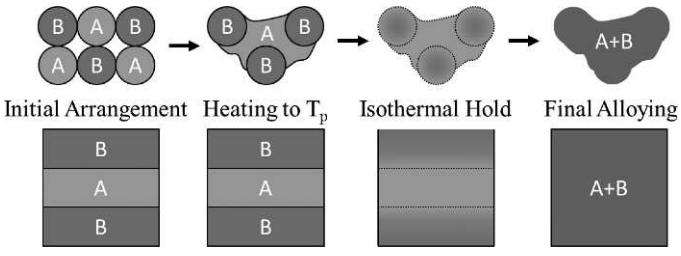


Fig. 1. Transient liquid phase sintering for a paste-based (above) and a layer based (below) system.

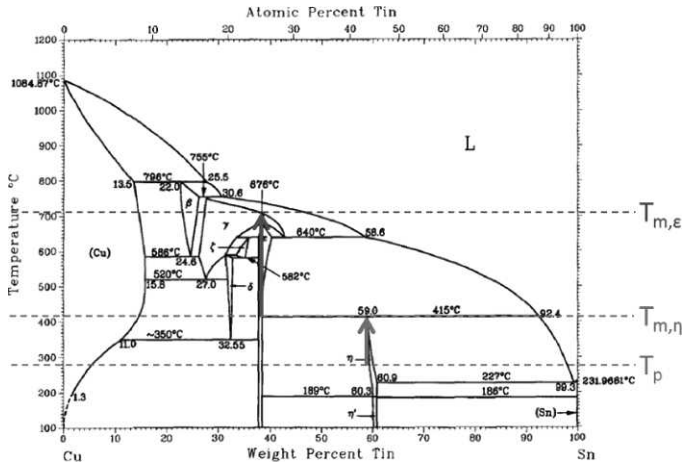


Fig. 2. The copper-tin system (cf. [22]).

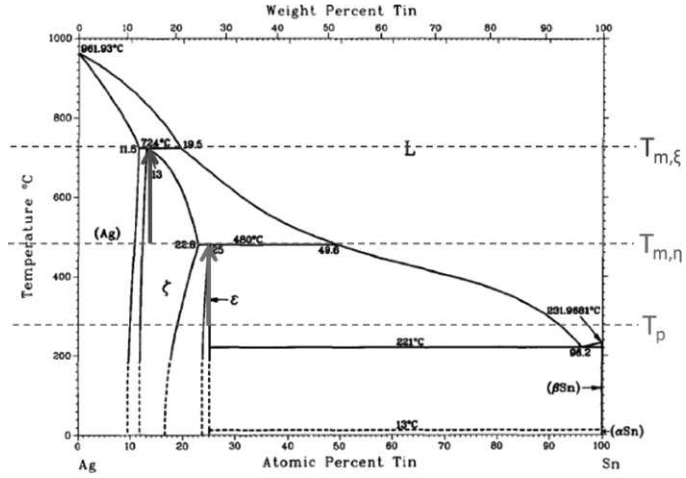


Fig. 3. The silver-tin system (cf. [23]).

melting point to 480°C occurs. At concentrations below 14.1%, the melting temperature can exceed 724°C.

### *B. Sinter Paste Design*

To prevent oxidation and corrosion of the metal particles, to ensure homogeneous particle distribution, and to enable stencil printability, the constituents were mixed in a flux binder to form a paste. The mixing procedure for a Cu-Sn sinter paste can be found in Fig. 4. The process steps can be described as follows:

1. Particles of constituent A and constituent B were weighed according to the required weight-percent ratio. This ratio was determined following the information from phase diagrams available in the literature.
2. A and B were mixed in a dry state until a homogenous mix of powders was achieved.
3. Organic liquids were mixed to form a fluxing binder to prevent particle oxidation and facilitate the sintering process.
4. The dry-mixed metal powders were blended with the binder to form a sinter paste.

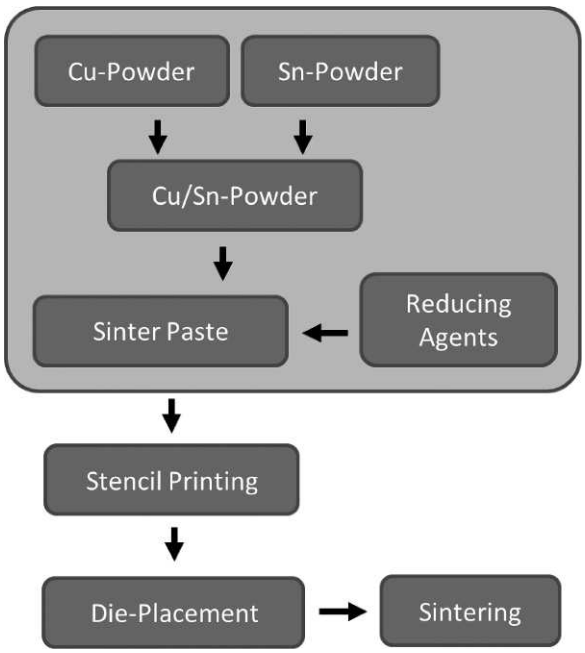


Fig. 4. Preparation of Cu-Sn pastes and shear test specimen.

To manufacture shear specimens, the following additional steps were performed:

5. Stencil printing of the sinter paste on a copper substrate.
6. Placement of a copper die onto the layer of stencil-printed sinter paste.
7. Pressure-less sintering of the shear test specimen assembly without vacuum or reducing atmosphere.

In addition to preventing oxidation of sinter paste particles, the binder also reduces oxides present on the metallized surfaces to be joined. The sinter pastes developed for this study are capable of activating Cu, Ag, and Ni surfaces and enabling good wetting behavior of the liquid Sn for these metallizations as well as for the Cu and Ag sinter paste particles. As Sn is used in both as the majority constituent of the liquid, the wetting capabilities of the sinter pastes are close to those of Sn-based solders.

One advantage of the sinter paste approach and the use of a fluxing binder is that no special treatment is required for conventional power and high temperature electronic metallization (Cu, Ni) in contrast to sintered silver, which requires a noble metal (Ag, Au, Pd) metallization. The organic binders are nontoxic, stable, and low cost. The raw material costs associated with Ag-Sn pastes are high due to the high amount of Ag, whereas the cost for Cu-Sn pastes is comparable to those of solders from the same constituents. The process time is longer than that of conventional solders, but the stencil printability enables manufacturing with established procedures and equipment. No vacuum, inert, or reducing atmosphere is required during processing, which is part of many reflow solder attach processes.

In the following, the composition of the sinter pastes is defined according to the atomic weight percentage of their metal constituents. The number before the last element denotes its amount in weight percent, the first element of the paste name

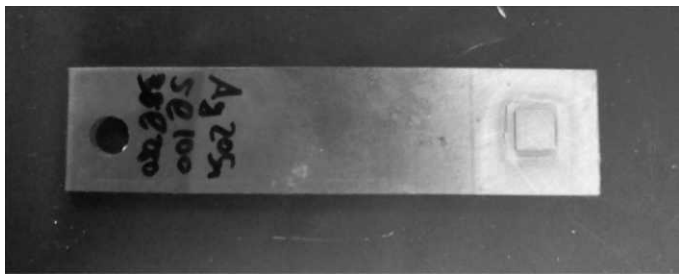

Fig. 5. Ag20Sn specimen for shear tests.

describes the balance. The pastes assessed in this study include Ag20Sn with 20 at.% Sn as well as Cu60Sn, Cu50Sn, and Cu40Sn with 60 at.%, 50 at.%, and 40 at.% Sn, respectively.

A top view of an Ag20Sn shear test specimen can be seen in Fig. 5. All specimens were manufactured by stencil printing a 100 μm thick layer through a square opening with a side length of 8.5 mm. The copper substrate plates had a length of 125 mm and width of 25 mm. A square copper die with a side length of 6.35 mm was placed on the sinter paste layer. The thickness of die and substrate were 3.2 mm and 1.6 mm, respectively; and the copper had a purity of 99.9%. To ensure a clean and smooth die and substrate surface, the joint surfaces were locally cleaned and smoothed with SiC grinding paper.

### *C. Process Progression and Microstructural Analyses*

Two approaches have been utilized in this study to assess and quantify the progression of the sintering process as a function of the process time (i.e., differential scanning calorimetry, DSC, and cross-sectioning).

During DSC analysis, one empty container and one with a test specimen are subjected to a constant temperature ramp rate, while the heat flow into each container is measured. When the test specimen undergoes a phase transformation, the heat flow into the test specimen is absorbed isothermally to provide the latent heat of transformation. The latent heat and the temperature of the phase transformation can be determined from the difference in the heat flow measured for the two samples during transformation, which appears as a deviation from a smooth curve.

A means to assess the progression of the sintering process is the analysis of the amount of residual low melting temperature phase to that of the high melting temperature phase due to IMC formation during the sintering process. The blue curve in Fig. 6 shows data from a DSC analysis run where the temperature was ramped from 30°C to 550°C at a constant ramp rate of 10°C per minute. Before each analysis run, the temperature was held at 30°C for 60 s to ensure that the system reached a state of equilibrium.

The small peak at approximately 221°C indicates the energy required to melt the eutectic Ag-Sn phase (cf. Fig. 3). The peak at 480°C correlates to the phase transformations occurring at this temperature level. The bumps at temperatures between approximately 300°C and 470°C indicate the phase transformations from the ε to the ξ phase during temperature rise at Sn concentrations of approximately 20-23%. The phases with these low levels of Sn also possess melting temperatures above 480°C. The ratio of the areas between the curves for high

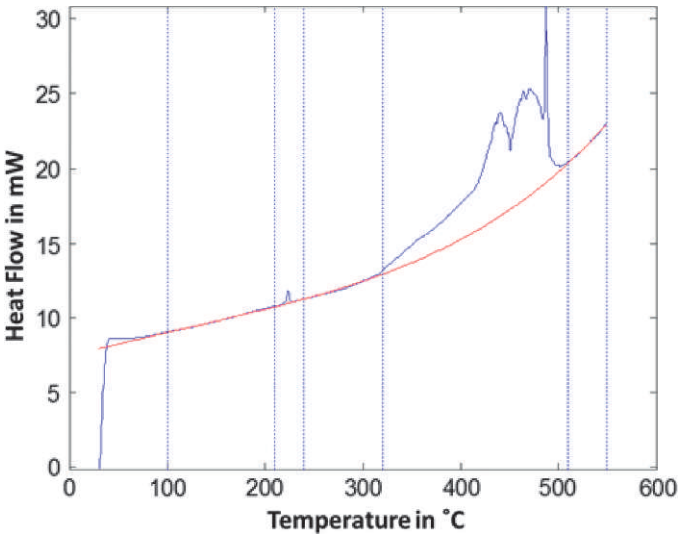


Fig. 6. DSC analysis run (blue) and a curve fit to the smooth parts of the curve (red) for a Ag20Sn paste during ramping from 30°C to 550°C.

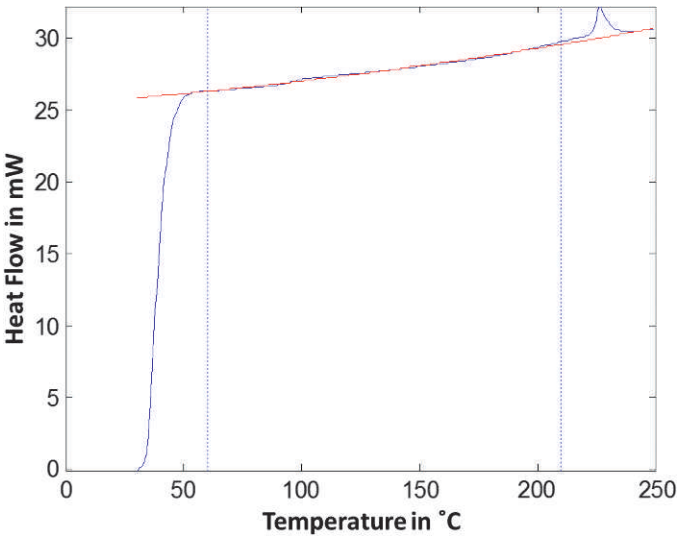


Fig. 7. DSC analysis run (blue) and a curve fit to the smooth parts of the curve (red) for a Ag20Sn paste during ramping from 30°C to 250°C and isothermal hold at 250°C.

melting temperature phase transformations and low melting temperature phase transformations can be calculated as an indicator for the process progression.

It is important to note that due to different masses of DSC specimen, the absolute heat flow varies significantly between different test runs. Therefore, relative quantities must be used to illustrate the convergence of the sintering process. Table III gives an overview of the process progression for the Ag20Sn paste after sintering for 5 and 10 min. It can be seen that after 5 min, 89.43% of the total area has converted to phases with high temperature transformations, whereas after 10 min, this ratio has increased to 99.34%. The main reason for this increase is the almost complete consumption of the low melting temperature eutectic Ag-Sn phase. This indicates that the sintering process for Ag20Sn sinter pastes is essentially completed after sintering times of less than 10 min.

An alternate approach that does not heat the sample all the way to the melting point of the IMC is shown in Fig. 7. Here a DSC analysis run is shown during which the temperature has been increased at a constant ramp rate from 30°C to 250°C, then held at this temperature for 150 s, and finally cooled back to 30°C, rapidly. Before each analysis run iteration, the temperature is held at 30°C for 60 s to ensure that a state of equilibrium is reached. The ramp rate for heating and cooling was set to 40°C per minute to reduce the influence of elevated temperatures during ramping on the annealing of the sinter joint.

Table III
Process Progression of a Ag20Sn Sinter Paste After 5 and 10 min of Sintering at 300°C

| Sinter time at 300°C | 5 min | 10 min |
|---|---|---|
| 221°C area | 6.517 | 0.475 |
| 480°C area | 55.141 | 71.809 |
| Total area | 61.658 | 72.208 |
| 480°C ratio | 89.43% | 99.34% |

Analogously to Fig. 6, the area of the bump at 221°C indicates the residual phase with low phase transition temperatures. When this test run is repeated multiple times, this bump area will decrease further until it is almost completely consumed.

A major advantage of this approach is that the specimen can be reused and the comparison between the calculated areas is consistent. Fig. 8 and Fig. 9 show the process progression for

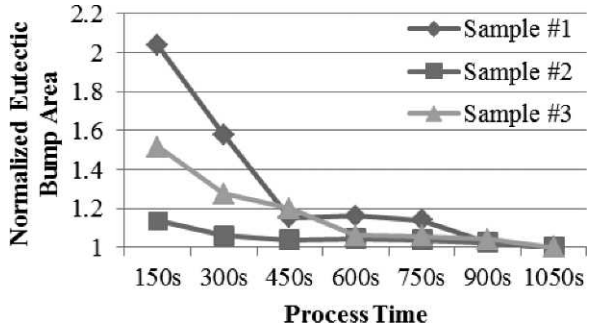


Fig. 8. Process progression after multiple runs as shown in Fig. 7. The three curves indicate three specimens of Ag20Sn paste from the same batch.

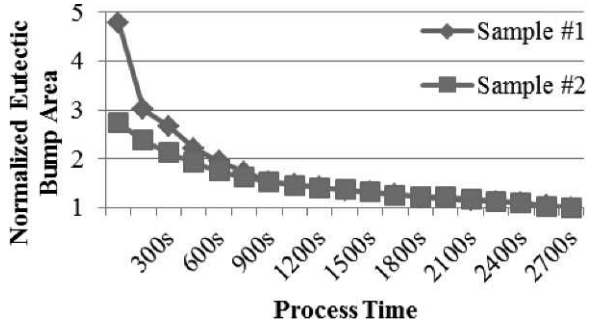


Fig. 9. Process progression for two specimens of Cu30Sn paste from the same batch.

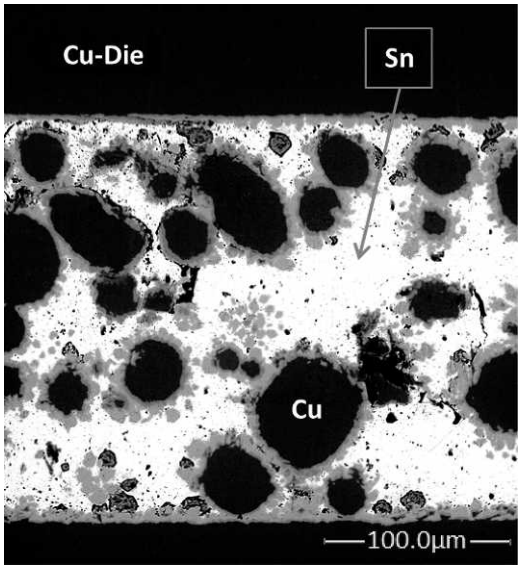


Fig. 10. Cross section of a Cu50Sn sinter joint after sintering at 280°C for 2.5 min.

multiple Ag20Sn and Cu30Sn specimens, respectively. All Ag20Sn samples were made from the same batch, as were all the Cu30Sn samples. It can be concluded that for the Ag20Sn pastes assessed, the process is completed after approximately 15 min. The Cu30Sn conversion has occurred after 15 min as well. This does not show, however, the conversion of $Cu_6Sn_5$ to $Cu_3Sn$ that will occur for extended annealing durations.

Cross sections of sintered Cu-Sn specimens have been used to verify the results found by the DSC analysis runs. Fig. 10 and Fig. 11 show cross sections of a Cu50Sn specimen after 2.5 and 30 min of sintering at 280°C, respectively, at 500× magnification.

It can be seen that for the shorter process time, the presence of intermetallic compounds is local; no bridging between die and substrate by IMCs is achieved. The joint annealed for 30 min shows bridging of die and substrate by IMCs and Cu particles, it consists primarily of Cu particles connected with IMCs; locally, residual solder is present. It should be noted that a thick joint thickness of 200 µm was used for these cross sections; still, the joint has predominately converted to IMCs after only 30 min. This is consistent with the process completion time shown by the DSC analyses for Cu-Sn specimen. Thinner joints might lead to further reduced process durations.

Furthermore, Fig. 11 shows localized void formation in the joint. It can be seen that a void is formed where Cu-particles are lacking. It is hypothesized that the liquid present here upon melting is drawn into cavities between Cu particles by capillary forces, and, as the mixture of liquid Sn and solid Cu interdiffuses, empty space is left behind.

EDS was utilized to analyze the compounds formed during processing of the sinter pastes. Fig. 12 shows a region of the same joint as in Fig. 11 at 2,500× magnification. Two spectra of the bright gray IMC, two of the dark gray IMC, and one spectrum of a Cu particle, have been analyzed. The results are given in Table IV.

In an SEM photomicrograph, Cu appears darker than Sn. With increasing Cu concentration, the compound darkness

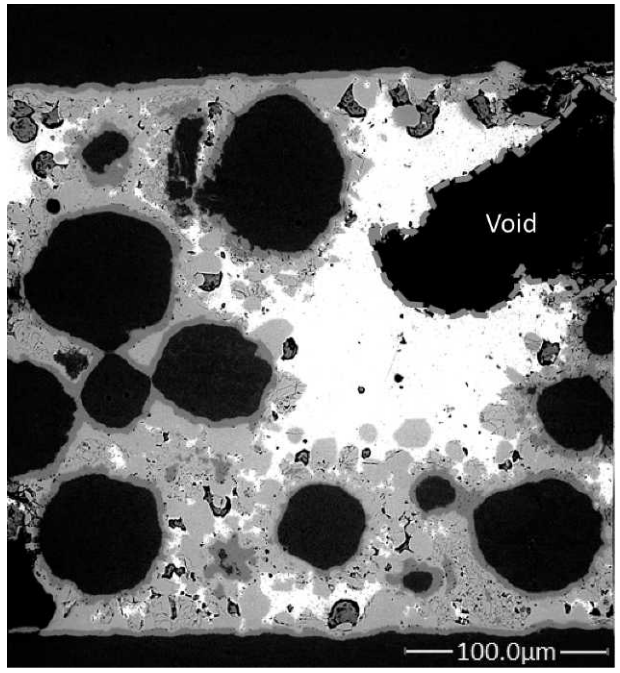


Fig. 11. Cross section of a Cu50Sn sinter joint after sintering for 30 min at 280°C.

increases. Therefore, the Cu concentration of spectra #1 and #2 should be lower than those of #3 and #4. The atomic weight percent of Cu for spectra #1 and #2 is 62.67 at.% and 62.11 at.%, respectively, which is relatively close to the 54.54 at.% that is ideally expected from the η-phase with a $Cu_6Sn_5$ stoichiometry (cf. Fig. 2).

The atomic weight percent of Cu for spectra #3 and #4 is 78.08 at.% and 78.01 at.%, respectively. This is in full agreement with what is expected from a $Cu_3Sn$ IMC correlating to the ε phase with an ideal Cu concentration of 75 at.%. The formation and growth of the Cu-Sn IMCs follows the

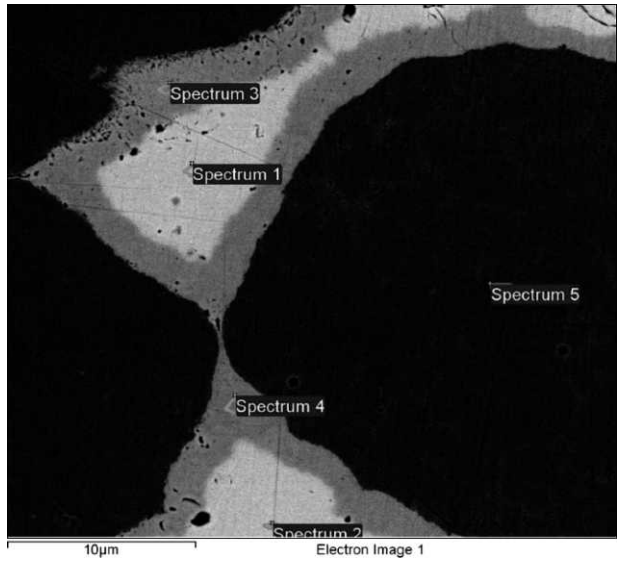


Fig. 12. Cross-sectional region used for EDS analyses of IMCs present in the sinter joint

Table IV
Summary of the EDS Analyses; Spectrum Locations Shown in Fig. 12

| Spectrum | Sn (at.%) | Cu (at.%) | Compound type |
|---|---|---|---|
| #1 | 37.33 | 62.67 | $Cu_6Sn_5$ (η phase) |
| #2 | 37.89 | 62.11 | $Cu_6Sn_5$ (η phase) |
| #3 | 21.92 | 78.08 | $Cu_3Sn$ (ε phase) |
| #4 | 21.99 | 78.01 | $Cu_3Sn$ (ε phase) |
| #5 | 3.27 | 96.73 | Cu |

known literature on IMC formation of Sn-based solders on Cu substrates.

The formation of IMCs throughout the joint during processing can also be visualized by EDS mapping. Fig. 13 shows the distribution of Sn and Cu atoms in the joints for process durations of 2.5 and 30 min. The change in distribution of atoms is best visible for Cu. After 2.5 min, the Cu atoms are concentrated within the spherical Cu particles and in the small (few μm) IMCs surrounding them. The diffusion of Cu into Sn during 30 min of processing leads to a more homogeneous atomic distribution. A continuous layer of Cu can be detected bridging die and substrate. Even though concentration gradients exist between the Cu particles and the IMCs, the joint structure is now much more homogeneous. The only exceptions to this are the voided areas and the associated Sn-rich area at the top corner, composed predominately of Sn.

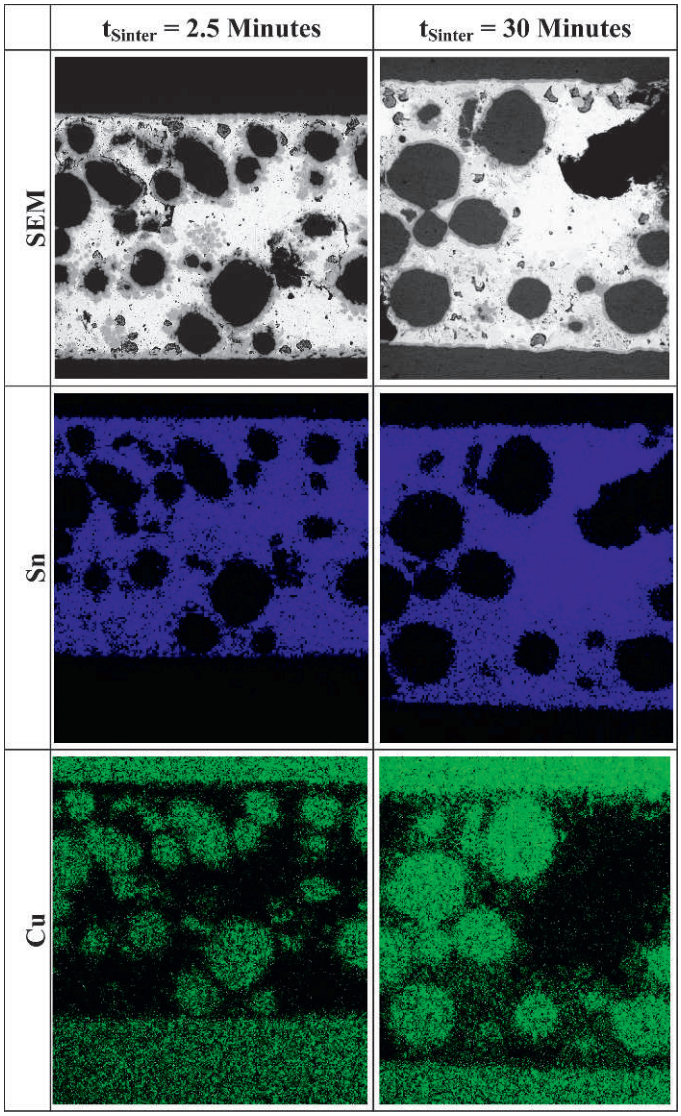


Fig. 13. Distribution of Sn (blue) and Cu (green) by EDS mapping after 2.5 min and 30 min of sintering. Note that $T_h > 1$ indicates that $T_m$ is exceeded under this condition.

### *D. Temperature-Dependent Shear Strength of Sinter Joints*

A test setup to enable shear strength characterization up to temperatures of 600°C was developed. It consists of a Tinius Olsen H25K-T benchtop universal testing machine, an oven that is thermally insulated from the environment by high temperature insulation wool, and a shear fixture. An image of the oven and the testing machine are shown in Fig. 14. During testing, the specimen is positioned within the shear fixture, the oven is closed, and the specimen is heated to the appropriate temperature. The shear test is then initiated and the specimens are sheared at a speed of 0.1 in.min.

Shear samples joined by Ag20Sn, Cu60Sn, Cu50Sn, and Cu40Sn sinter paste were prepared. They were sheared at temperatures of 25°C, 125°C, 250°C, 400°C, and 600°C. Fig. 15 gives an overview of the shear strength of Ag20Sn shear specimens for different temperatures. It can be seen that the shear strength is relatively constant up to 400°C and drops


Fig. 14. High temperature shear test system: integration of a miniature oven in a benchtop testing machine.

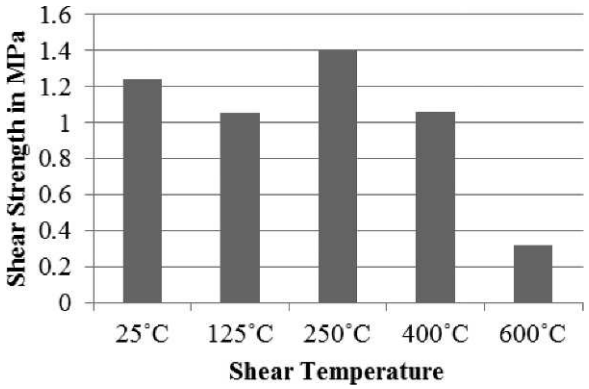


Fig. 15. Shear strength of Ag20Sn specimen.

significantly at 600°C. This behavior is consistent with the phase diagram shown in Fig. 3, where the dominant IMC phase has a melting temperature of 480°C.

After initial testing with one sample per temperature condition, it could be seen that the shear strength of the Cu-Sn specimen, as will be discussed shortly, is approximately one order of magnitude higher than that of Ag20Sn specimen. The decision was therefore made to focus in this study on the shear strength assessment of Cu-Sn joints with high shear strengths adequate for an interconnect application in electronic systems.

The sample size for the Cu-Sn shear tests was five for each data point. As can be seen, the shear strength varies significantly for individual test points. Yet the level of variation between different batches is consistent; and the results are comparable and repeatable. Fig. 16 depicts the shear strength of Cu60Sn specimens for different temperatures. It can be seen that the shear strength drops considerably at 400°C. This indicates that the joint is dominated by low melting temperature phases.

Fig. 17 shows the shear strength of Cu50Sn specimens. The joints possess high strength up to 400°C but reduced strength of approximately 3.6 MPa at 600°C. It can be concluded that the dominant phase in this joint is the η phase ($Cu_6Sn_5$) with a melting temperature of 415°C. This is consistent with the microstructures of Cu50Sn sinter joints that consist of $Cu_6Sn_5$ as the dominant IMC. It is furthermore interesting to note the increased strength at 400°C compared with ambient temperature, which may be due to additional annealing homogenizing the joint.

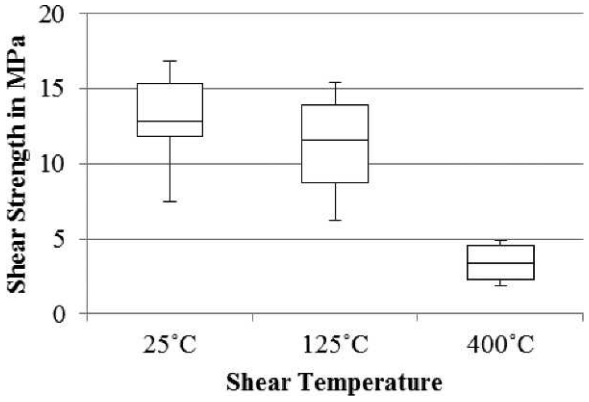


Fig. 16. Shear strength of Cu60Sn specimen.

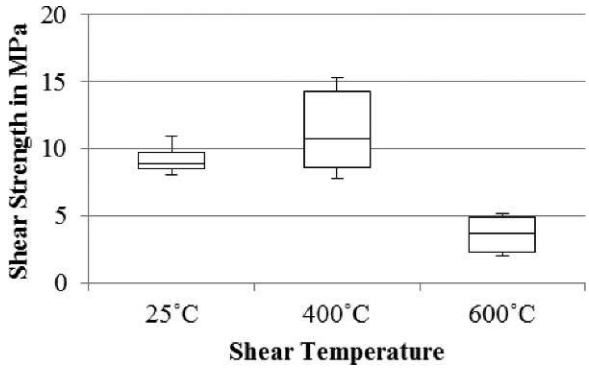


Fig. 17. Shear strength of Cu50Sn specimen.

Fig. 18 summarizes the shear strength of Cu40Sn joints. It can be seen that the joints possess high strength over the entire temperature range. This indicates that the joint consists predominately of ε ($Cu_3Sn$) IMCs. Again, the shear strength at 400°C is higher than that under ambient temperatures for the same reasons as for the Cu50Sn paste. This material shows potential for application temperatures up to 600°C.

Fig. 19 summarizes the shear strength of the Cu-Sn sinter pastes assessed in this study. It can be seen that Cu60Sn pastes are not feasible for high temperature applications; Cu50Sn can be used up to 400°C, and Cu40Sn pastes show the potential for

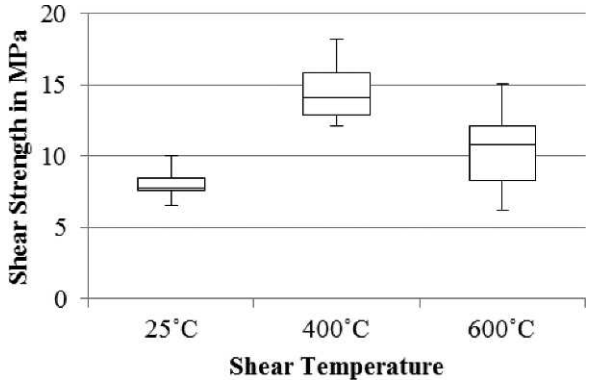


Fig. 18. Shear strength of Cu40Sn specimen.

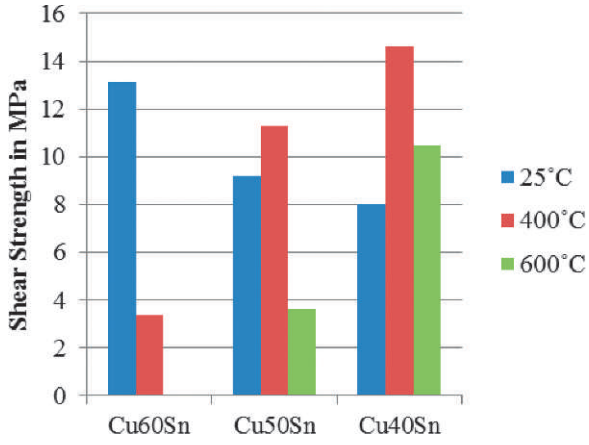


Fig. 19. Shear strength of the different Cu-Sn pastes at 25°C, 400°C, and 600°C.

use up to 600°C. As the processing of pastes with low ratios of low melting temperature constituent leads to higher voiding, the shear strength at ambient temperature is highest for the Cu60Sn pastes. At 400°C, the Cu50Sn paste shows the highest strength, and at 600°C, the Cu40Sn paste performs best.

## Conclusions

Pastes have been developed that enable pressure-less sintering without a vacuum or reducing atmosphere for the low temperature joining of electronic components. Differential scanning calorimetry (DSC) and cross sections were used to determine the time for sinter process completion. It was shown that the transformation of these pastes reaches completion after approximately 15 min of processing at 280°C. The shear strength of Ag-Sn and Cu-Sn sinter joints at temperatures of 25°C, 125°C, 250°C, 400°C, and 600°C was assessed. It was demonstrated that the strength of Ag20Sn joints does not decrease up to temperatures of 400°C. The Cu-Sn system can be used to form high strength joints robust to temperature levels of 600°C.

## Acknowledgments

The authors would like to thank the over 50 members of the Center for Advanced Life Cycle Engineering (CALCE) at the University of Maryland for their support of this work.

## References

[1] F. McCluskey, R. Grzybowski, and T. Podlesak, *High Temperature Electronics*, CRC Press, Boca Raton, FL, 1997.

[2] J. Casady and J.R.U. Dillard, "A hybrid 6H-SiC temperature sensor operational from 25°C to 500°C," *IEEE Transactions on Components Packaging & Manufacturing Technology Part A*, Vol. 19, No. 3, pp. 416-422, 1996.

[3] T. Funaki, A. Kashyap, H. Mantooth, J. Balda, F. Barlow, T. Kimoto, and T. Hikihara, "Characterization of SiC diodes in extremely high temperature ambient," Proceedings of the 21st Annual IEEE Applied Power Conference and Exposition, APEC, 2006.

[4] P. Chauhan, M. Osterman, S. W. R. Lee, and M. Pecht, "Critical review of the Engelmaier model for solder joint creep fatigue reliability," *IEEE Transactions on Components and Packaging Technologies*, Vol. 32, No. 3, pp. 693-700, 2009.

[5] X. Deng, N. Chawla, and M. Koopman, "Deformation behavior of (Cu, Ag)-Sn intermetallics by nanoindentation," *Acta Materialia*, Vol. 52, pp. 4291-4303, 2004.

[6] T. Siewert, S. Liu, D. R. Smith, and J. C. Madeni, "Database for solder properties with emphasis on new lead-free solders—Properties of lead-free solders, Release 4.0," National Institute of Standards and Technology (NIST) and Colorado School of Mines, 2002.

[7] W.W. Gerberich, W.M. Mook, C. Carter, and R. Ballarini, "A crack extension force correlation for hard materials," *International Journal of Fracture*, Vol. 148, No. 2, pp. 109-144, 2007.

[8] J. Bai, Z.Z. Zhang, J.N. Calata, and G.-Q. Lu, "Low-temperaature sintered nanoscale silver as a novel semiconductor device-metallized substrate interconnect material," *IEEE Transactions on Components and Packaging Technologies*, Vol. 29, No. 3, pp. 589-593, 2006.

[9] H. Schwarzbauer and R. Kuhnert, "Novel large area joining technique for improved power device performance," *Conference Record of the 1989 IEEE Industry Applications Society Annual Meeting,* vol. 2, pp. 1348-1351, 1989.

[10] G.-Q. Lu, M. Zhao, G. Lei, J. Calata, X. Chen, and S. Luo, "Emerging leaf-free, high-temperature die-attach technology enabled by low-temperature sintering of nanoscale silver particles," International Conference on Electronic Packaging Technology & High Density Packaging, pp. 461-466, 2009.

[11] S. Kraft, A. Schletz, and M. Maerz, "Reliability of silver sintering on DBC and DBA substrates for power electronic applications," Proceedings of the 7th International Conference on Integrated Power Electronics Systems (CIPS), 2012.

[12] Y. Mei, G.-Q. Lu, X. Chen, S. Luo, and D. Ibitayo, "Migration of sintered nanosilver die-attach material on alumina substrate between 250°C and 400°C in dry air," *IEEE Transactions on Device and Materials Reliability*, Vol. 11, No. 2, pp. 316-322, 2011.

[13] P. Quintero and F. McCluskey, "Temperature cycling reliability of high-temperature lead-free die-attach technologies," *IEEE Transactions on Device and Materials Reliability*, Vol. 11, No. 4, pp. 531-539, 2011.

[14] K. Aasmundtveit, T. Luu, H.-V. Nguyen, R. Johannessen, N. Hoivik, and K. Wang, "Au-Sn fluxless SLID bonding: Effect of bonding temperature for stability at high temperature, above 400 °C," Proceedings of the 3rd Electronic Systems-Integration Technology Conference (ESTC), 2010.

[15] H. Mustain, W. Brown, and S. Ang, "Transient liquid phase die attach for high-temperature silicon carbide power devices," *IEEE Transactions on Components and Packaging Technologies*, Vol. 33, No. 3, pp. 563-570, 2010.

[16] R. Chuang and C. Lee, "Silver-indium joints produced at low temperatures for high temperature devices," *IEEE Transactions on Components and Packaging Technologies*, Vol. 25, No. 3, pp. 453-458, 2002.

[17] K. Guth, N. Oeschler, L. Boewer, R. Speckels, G. Strotmann, N. Heuck, S. Krasel, and A. Ciliox, "New assembly and interconnect technologies for power modules," Proceedings of the 7th International Conference on Integrated Power Electronics Systems (CIPS), 2012.

[18] S.W. Yoon, K. Shiozaki, S. Yasuda, and M. Glover, "Highly reliable nickel-tin transient liquid phase bonding technology for high temperature operational power electronics in electrified vehicles," Proceedings of the 27th Annual IEEE Applied Power Electronics Conference and Exposition (APEC), pp. 478-482, 2012.

[19] J.S. Kang, R.A. Gagliano, G. Ghosh, and M.E. Fine, "Isothermal solidification of Cu/Sn diffusion couples to form thin-solder joints," *Journal of Electronic Materials*, Vol. 31, No. 11, pp. 1238-1243, 2002.

[20] C. Ehrhardt, M. Hutter, H. Oppermann, and K.-D. Lang, "Transient liquid phase soldering for lead-free joining of power electronic modules in high temperature applications," Proceedings of the IMAPS High Temperature Electronics Conference (HiTEC), 2012.

[21] P. Quintero and F. McCluskey, "Silver-indium transient liquid phase sintering for high temperature die attachment," *Journal of Microelectronics and Electronic Packaging*, Vol. 6, pp. 66-74, 2009.

[22] N. Saunders and A. Miodownik, "The Cu-Sn (copper-tin) system," *Bulletin of Alloy Phase Diagrams*, Vol. 11, No. 3, pp. 278-285, 1990.

[23] I. Karakaya and W.T. Thompson, "The Ag-Sn (silver-tin) system," *Bulleting of Alloy Phase Diagrams*, Vol. 8, No. 4, pp. 340-347, 1987.